arXiv:2207.11967v1 [hep-ex] 25 Jul 2022

Search for dark matter-nucleon interactions via Migdal effect with DarkSide-50

P. Agnes,[1] I.F.M. Albuquerque,[2] T. Alexander,[3] A.K. Alton,[4] M. Ave,[2] H.O. Back,[3] G. Batignani,[5,6] K. Biery,[7] V. Bocci,[8] W.M. Bonivento,[9] B. Bottino,[10,11] S. Bussino,[12,13] M. Cadeddu,[9] M. Cadoni,[14,9] F. Calaprice,[15] A. Caminata,[11] M.D. Campos,[16] N. Canci,[17] M. Caravati,[9] M. Cariello,[11] M. Carlini,[17,18] M. Carpinelli,[19,20] V. Cataudella,[21,22] P. Cavalcante,[23,17] S. Cavuoti,[21,22] S. Chashin,[24] A. Chepurnov,[24] C. Cicalò,[9] G. Covone,[21,22] D. D'Angelo,[25,26] S. Davini,[11] A. De Candia,[21,22] S. De Cecco,[8,27] G. De Filippis,[21,22] G. De Rosa,[21,22] A.V. Derbin,[28] A. Devoto,[14,9] M. D'Incecco,[17] C. Dionisi,[8,27] F. Dordei,[9] M. Downing,[29] D. D'Urso,[19,20] M. Fairbairn,[16] G. Fiorillo,[21,22] D. Franco,[30] F. Gabriele,[9] C. Galbiati,[15,18,17] C. Ghiano,[17] C. Giganti,[31] G.K. Giovanetti,[15] A.M. Goretti,[17] G. Grilli di Cortona,[32] A. Grobov,[33,34] M. Gromov,[24,35] M. Guan,[36] M. Gulino,[37,20] B.R. Hackett,[3] K. Herner,[7] T. Hessel,[30] B. Hosseini,[9] F. Hubaut,[38] E.V. Hungerford,[39] An. Ianni,[15,17] V. Ippolito,[8] K. Keeter,[40] C.L. Kendziora,[7] M. Kimura,[41] I. Kochanek,[17] D. Korablev,[35] G. Korga,[39,17] A. Kubankin,[42] M. Kuss,[5] M. La Commara,[21,22] M. Lai,[14,9] X. Li,[15] M. Lissia,[9] G. Longo,[21,22] O. Lychagina,[35,24] I.N. Machulin,[33,34] L.P. Mapelli,[43] S.M. Mari,[12,13] J. Maricic,[44] C.J. Martoff,[45] A. Messina,[8,27] R. Milincic,[44] J. Monroe,[1] M. Morrocchi,[5,6] X. Mougeot,[46] V.N. Muratova,[28] P. Musico,[11] A.O. Nozdrina,[33,34] A. Oleinik,[42] F. Ortica,[47,48] L. Pagani,[49] M. Pallavicini,[10,11] L. Pandola,[20] E. Pantic,[49] E. Paoloni,[5,6] K. Pelczar,[17,50] N. Pelliccia,[47,48] S. Piacentini,[8] E. Picciau,[14,9] A. Pocar,[29] D.M. Poehlmann,[49] S. Pordes,[7] S.S. Poudel,[39] P. Pralavorio,[38] D.D. Price,[51] F. Ragusa,[25,26] M. Razeti,[9] A. Razeto,[17] A.L. Renshaw,[39] M. Rescigno,[8] J. Rode,[31,30] A. Romani,[47,48] D. Sablone,[15,17] O. Samoylov,[35] W. Sands,[15] S. Sanfilippo,[13,12] E. Sanford,[51] C. Savarese,[15] B. Schlitzer,[49] D.A. Semenov,[28] A. Shchagin,[42] A. Sheshukov,[35] M.D. Skorokhvatov,[33,34] O. Smirnov,[35] A. Sotnikov,[35] S. Stracka,[5] Y. Suvorov,[21,22,33] R. Tartaglia,[17] G. Testera,[11] A. Tonazzo,[30] E.V. Unzhakov,[28] A. Vishneva,[35] R.B. Vogelaar,[23] M. Wada,[15,41] H. Wang,[43] Y. Wang,[43,36] S. Westerdale,[15,9] M.M. Wojcik,[50] X. Xiao,[43] C. Yang,[36] and G. Zuzel[50]

(The DarkSide Collaboration)

[1] *Department of Physics, Royal Holloway University of London, Egham TW20 0EX, UK*
[2] *Instituto de Física, Universidade de São Paulo, São Paulo 05508-090, Brazil*
[3] *Pacific Northwest National Laboratory, Richland, WA 99352, USA*
[4] *Physics Department, Augustana University, Sioux Falls, SD 57197, USA*
[5] *INFN Pisa, Pisa 56127, Italy*
[6] *Physics Department, Università degli Studi di Pisa, Pisa 56127, Italy*
[7] *Fermi National Accelerator Laboratory, Batavia, IL 60510, USA*
[8] *INFN Sezione di Roma, Roma 00185, Italy*
[9] *INFN Cagliari, Cagliari 09042, Italy*
[10] *Physics Department, Università degli Studi di Genova, Genova 16146, Italy*
[11] *INFN Genova, Genova 16146, Italy*
[12] *INFN Roma Tre, Roma 00146, Italy*
[13] *Mathematics and Physics Department, Università degli Studi Roma Tre, Roma 00146, Italy*
[14] *Physics Department, Università degli Studi di Cagliari, Cagliari 09042, Italy*
[15] *Physics Department, Princeton University, Princeton, NJ 08544, USA*
[16] *Physics, Kings College London, Strand, London WC2R 2LS, UK*
[17] *INFN Laboratori Nazionali del Gran Sasso, Assergi (AQ) 67100, Italy*
[18] *Gran Sasso Science Institute, L'Aquila 67100, Italy*
[19] *Chemistry and Pharmacy Department, Università degli Studi di Sassari, Sassari 07100, Italy*
[20] *INFN Laboratori Nazionali del Sud, Catania 95123, Italy*
[21] *Physics Department, Università degli Studi "Federico II" di Napoli, Napoli 80126, Italy*
[22] *INFN Napoli, Napoli 80126, Italy*
[23] *Virginia Tech, Blacksburg, VA 24061, USA*
[24] *Skobeltsyn Institute of Nuclear Physics, Lomonosov Moscow State University, Moscow 119234, Russia*
[25] *Physics Department, Università degli Studi di Milano, Milano 20133, Italy*
[26] *INFN Milano, Milano 20133, Italy*
[27] *Physics Department, Sapienza Università di Roma, Roma 00185, Italy*
[28] *Saint Petersburg Nuclear Physics Institute, Gatchina 188350, Russia*
[29] *Amherst Center for Fundamental Interactions and Physics Department, University of Massachusetts, Amherst, MA 01003, USA*

[30] *APC, Université de Paris, CNRS, Astroparticule et Cosmologie, Paris F-75013, France*
[31] *LPNHE, CNRS/IN2P3, Sorbonne Université, Université Paris Diderot, Paris 75252, France*
[32] *INFN Laboratori Nazionali di Frascati, Frascati 00044, Italy*
[33] *National Research Centre Kurchatov Institute, Moscow 123182, Russia*
[34] *National Research Nuclear University MEPhI, Moscow 115409, Russia*
[35] *Joint Institute for Nuclear Research, Dubna 141980, Russia*
[36] *Institute of High Energy Physics, Beijing 100049, China*
[37] *Engineering and Architecture Faculty, Università di Enna Kore, Enna 94100, Italy*
[38] *Centre de Physique des Particules de Marseille, Aix Marseille Univ, CNRS/IN2P3, CPPM, Marseille, France*
[39] *Department of Physics, University of Houston, Houston, TX 77204, USA*
[40] *School of Natural Sciences, Black Hills State University, Spearfish, SD 57799, USA*
[41] *AstroCeNT, Nicolaus Copernicus Astronomical Center, 00-614 Warsaw, Poland*
[42] *Radiation Physics Laboratory, Belgorod National Research University, Belgorod 308007, Russia*
[43] *Physics and Astronomy Department, University of California, Los Angeles, CA 90095, USA*
[44] *Department of Physics and Astronomy, University of Hawai'i, Honolulu, HI 96822, USA*
[45] *Physics Department, Temple University, Philadelphia, PA 19122, USA*
[46] *Université Paris-Saclay, CEA, List, Laboratoire National Henri Becquerel (LNE-LNHB), F-91120 Palaiseau, France*
[47] *Chemistry, Biology and Biotechnology Department, Università degli Studi di Perugia, Perugia 06123, Italy*
[48] *INFN Perugia, Perugia 06123, Italy*
[49] *Department of Physics, University of California, Davis, CA 95616, USA*
[50] *M. Smoluchowski Institute of Physics, Jagiellonian University, 30-348 Krakow, Poland*
[51] *The University of Manchester, Manchester M13 9PL, United Kingdom*

(Dated: July 26, 2022)

Dark matter elastic scattering off nuclei can result in the excitation and ionization of the recoiling atom through the so-called Migdal effect. The energy deposition from the ionization electron adds to the energy deposited by the recoiling nuclear system and allows for the detection of interactions of sub-GeV/c^2 mass dark matter. We present new constraints for sub-GeV/c^2 dark matter using the dual-phase liquid argon time projection chamber of the DarkSide-50 experiment with an exposure of $(12\,306 \pm 184)$ kg d. The analysis is based on the ionization signal alone and significantly enhances the sensitivity of DarkSide-50, enabling sensitivity to dark matter with masses down to 40 MeV/c^2. Furthermore, it sets the most stringent upper limit on the spin independent dark matter nucleon cross section for masses below 3.6 GeV/c^2.

The presence of dark matter (DM) in the universe is strongly supported by many observations [1–3], based only on DM gravitational effects. Other possible interactions remain unknown. Weakly interacting massive particles are theoretically-favored DM candidates with masses in the GeV/c^2–TeV/c^2 range [4]. Attempts to detect DM elastic scattering off target nuclei have resulted in strong limits on DM interactions for masses above a few GeV/c^2 [5–8]. Furthermore, several mechanisms that explain the observed DM density point to light DM particles (LDM), with masses in the sub-GeV/c^2 range [9, 10].

LDM is difficult to probe with direct detection experiments because the DM-induced nuclear recoil (NR) energy is generally below the detection threshold. However, atomic effects modeled by Migdal [11] predict emission of electrons associated with a fraction of nuclear recoils. This electron recoil (ER) component, in addition to the NR one, increases the probability of exceeding the detection threshold, thus opening a window of exploration for DM particles with masses down to a few tens of MeV/c^2. The idea by Migdal originated in the context of nuclear physics for alpha and beta emissions [12–15], and has been recently adapted to direct dark matter experiments [16–29].

In this Letter, we report the results of a search for LDM-nucleon elastic interactions based on the ionization signal in the DarkSide-50 (DS-50) detector, taking into account the extra energy detected due to the Migdal effect (ME). Previous DM searches including the ME were performed by several Collaborations [30–34].

DS-50 uses a dual-phase liquid argon (LAr) time projection chamber (TPC), located at the INFN Laboratori Nazionali del Gran Sasso (LNGS) in Italy. Particle interactions in the 46.4±0.7 kg active target induce scintillation pulses (S1) and ionization electrons. The latter are drifted through an electric field up to the gas pocket, at the top of the TPC, where they produce a secondary pulse of light (S2) by electroluminescence. S1 and S2 ultraviolet photons are converted into the visible range by tetraphenyl butadiene, a wavelength shifter that coats the inner surfaces of the TPC. Visible photons are detected by two arrays of 19 3-in photomultipli-

ers, one located above the anode and one below the cathode, respectively. The TPC is installed at the center of a stainless-steel sphere, filled with 30 t of boron-loaded liquid scintillator, which is in turn installed in a cylindrical tank, filled with 1 kt of ultrapure water. The scintillator and water detectors are equipped with PMTs, and act as neutron and muon veto, respectively. More details on the detector can be found in ref. [5, 35–38].

We perform this analysis using the 653.1 live-days DS-50 dataset, from December 12, 2015 to October 4, 2017. We use the ionization signal S2 since it has significantly lower detection threshold than S1 thanks to the gain of the electroluminescence. The region of interest (ROI) is defined as where the ionization response is calibrated [39] and backgrounds are well-understood. We characterize the strength of the ionization signal by the number of electrons that are extracted into the gas-region at the top of the TPC. Given the electric field settings of the TPC, the extraction efficiency for electrons from the liquid into the gas is essentially 100% and so N_e is a good measure of the ionization signal. This corresponds to the number N_e of electrons counted in S2 within $[4, 170]$, equivalent to $[0.06, 21]$ $\mathrm{keV_{er}}$ ($[0.64, 288]$ $\mathrm{keV_{nr}}$) in the ER (NR) energy scale. Above $4e^-$, the contribution of spurious electrons, captured by impurities along their drift and re-emitted with a delay, to the background model is negligible [40].

We consider only single-scatter events. Such events are identified by requiring a single valid S2 pulse. The extra S2 pulses induced by electrons extracted from the cathode by the UV photons from S1 or S2 pulses are identified as echoes by their timing and not counted. A set of quality cuts, based on the topological distribution and the time profile of the S2 signal, and on S2/S1, is implemented to reject events with overlapping pulses without appreciable loss of acceptance, as described in Ref. [40]. An additional set of selection cuts is applied to remove spurious S2 pulses mainly induced by electrons captured by impurities, events with an echo from surface alphas that lose normal S2 to the TPC wall, and pile up events, associated to random coincidences between very low S1 and S2 pulses from the anode. The final data-set accounting for the quality and selection cuts corresponds to an exposure of $(12\,306 \pm 184)$ kg d.

The major sources of background events in the ROI considered in the background calculation are ^{39}Ar and ^{85}Kr decays occurring in the LAr bulk (internal background) and γ-rays and X-rays from radioactive contaminants in the PMTs and stainless-steel cryostat (external background). Backgrounds originating from radiogenic and cosmogenic neutrons, as well as coherent elastic neutrino-nucleus scattering from solar and atmospheric neutrinos, are negligible in comparison. The main systematic uncertainties for the internal background stem from the atomic exchange, screening effects, and ionization response. A subdominant systematic uncertainty from the Q-value is also included [41]. The systematic uncertainties and their impact are discussed in detail in [40]. Uncertainties on the external background are due to the detector response and from Monte Carlo statistics. More details on the event selection and background models are described in [40].

The calibration of the detector and its response to ER and NR energy deposits has been performed in [39]. The ionization response to electronic recoils has been measured down to 180 eV_{er} and a fit to the data with a function of the Thomas-Imel box model form allows an extrapolation down to $\mathcal{O}(100\,\mathrm{eV})$. Similarly, the expected number of ionization electrons for NR is given by the Thomas-Imel box model, where the number of electron-ion pairs is obtained with Bezrukov's model [42] and with the Ziegler et al. model for the nuclear screening function [43]. The ionization response to NR has been measured down to 500 eV_{nr}. This is the lowest threshold ever reached in liquid argon and corresponds to 3 ionization electrons. The ER and NR ionization models are constrained by fitting the ^{241}Am^{9}Be and ^{241}Am^{13}C neutron sources data, β-decay data of ^{39}Ar, and electron captures of ^{37}Ar obtained during the DS-50 calibration campaign, and by external datasets from the SCENE [44], ARIS [45] and Joshi *et al.* [46] experiments. Details can be found in [39].

The elastic scattering of a DM particle off an argon nucleus at rest induces an instantaneous momentum change of the nucleus with respect to the atomic electrons, resulting in the possible ionization or excitation of the atom: this is the ME. When considering the ME, both NR and ER signals are present. For the first time, we consider and sum both contributions to the predicted signal. Finally, in the signal model we consider only electron energy injections originating from single ionization since double ionization or excitation probabilities are negligible.

The differential event rate for DM elastically scattering on an argon nucleus with respect to the nuclear recoil energy E_{nr} and DM velocity v is given by

$$\frac{d^2 R_{\mathrm{nr}}}{dE_{\mathrm{nr}}\, dv} = \frac{\rho_{DM}\, \sigma_{SI}}{2\, \mu_N^2\, m_{DM}} \frac{f(v)}{v}, \qquad (1)$$

where $\rho_{DM} = 0.3$ GeV cm^{-3} c^{-2} is the local DM

density, m_{DM} is its mass, σ_{SI} is the DM-nucleus spin independent scattering cross section, μ_N is the DM-nucleus reduced mass, and $f(v)$ is the DM speed distribution in the laboratory frame. We assume the Standard Halo Model with a DM escape velocity $v_{esc} = 544$ km/s, and local standard of rest velocity $v_0 = 238$ km/s [47].

The rate for a nuclear recoil energy $E_{\rm nr}$, accompanied by an ionization electron with energy E_{er} is given by [17]

$$\frac{d^2R}{dE_{\rm nr}\,dE_{\rm er}} = \frac{dR_{\rm nr}}{dE_{\rm nr}}\frac{1}{2\pi}\sum_{n,\ell}\frac{dp^c_{q_e}(n\ell \to E_{\rm er})}{dE_{\rm er}}, \qquad (2)$$

where $dR_{\rm nr}/dE_{\rm nr}$ is the standard DM nuclear recoil rate, $p^c_{q_e}$ is the probability to emit an electron from the (n,ℓ) shell with final energy $E_{\rm er}$, $q_e = m_e\sqrt{2E_{nr}/m_N}$ is the electron momentum in the nucleus rest frame immediately after the DM interaction, m_e is the electron mass, and m_N is the nucleus mass. Since the emitted electron may come from an inner orbital, the remaining excited state will immediately release further energy in the form of additional electrons or photons. These are measured simultaneously with the energy deposited by the initial ionization electron. As a consequence, the total energy deposited in the electromagnetic channel can be estimated to be $E_{EM} = E_{\rm er} + E_{n\ell}$, where $E_{n\ell}$ is the binding energy of the $(n,\,\ell)$ state. In this analysis, we use the differential probabilities for isolated Ar atoms computed in [17], and we consider the ionization contributions of all the electron shells. In Ref. [24] it has been shown that the prediction of Ref. [17] for the probability of emitting an electron from the valence shell in isolated argon atoms is robust. However, in liquid argon, the valence shell shows a band structure and a reduced binding energy. Neglecting this difference in the computation results in a smaller ionization probability [48], thus reducing the predicted ME signal event yield. The double differential rate in Eq. (2) for two representative DM masses (0.36 GeV/c^2 and 1.49 GeV/c^2) as a function of E_{EM} and $E_{\rm nr}$ are shown in Figure 1, along with the corresponding 1D integrated distributions in the ME electron and the NR channels. The peaks in the ME electron spectrum correspond to the contribution of the different atomic shells. The total energy deposited in the detector E_d is the sum of the nuclear and electromagnetic contributions: $E_d = E_{\rm nr} + E_{EM}$.

The signal for spin independent DM-nucleon scattering is modeled with a Monte Carlo approach simulating a combined NR (recoiling atom) and ER (ionization electron from the ME) event using Eq. 2.

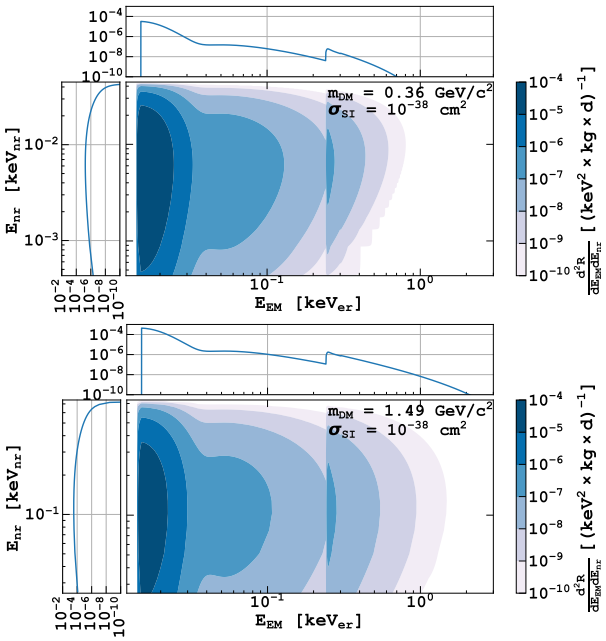


FIG. 1. Double differential ionization rate as a function of the nuclear recoil energy ($E_{\rm nr}$) and electromagnetic channel energy ($E_{\rm EM}$) is shown for two representative DM masses, 0.36 GeV/c^2 (top) and 1.49 GeV/c^2 (bottom). The rate is given in events/(keV^2 kg d) and covers E_{EM} from 0.01 to 3 keV and E_{nr} from $4\cdot10^{-4}$ to $4\cdot10^{-2}$ keV for a DM mass of 0.36 GeV/c^2 and E_{nr} from $2.5\cdot10^{-2}$ to $7.5\cdot10^{-1}$ keV for a particle of mass 1.49 GeV/c^2. The top and side panels of each figure depict the corresponding integrated distributions in the ME electron (top panels) and the NR (left panels) channels.

The detector response model is applied separately to the electrons generated from NR and ER.

When the primary Migdal ionization involves an inner shell electron ($n = 1$ or $n = 2$), the binding energy $E_{n\ell}$ ($E_{1s} = 3.2$ keV, $E_{2s} = 300$ eV and $E_{2p} = 240$ eV) is released via subsequent X-ray/Auger cascades. Given the non-linearity of the calibration NR and ER yield functions, the expected deposited energy is sensitive to the number of these subsequent ionizing emissions. Despite this, we calculate the ME electron yield as from a single ER energy deposit. This choice is conservative, as the ionization yield monotonically decreases with recoil energy. We tested this assumption against an alternative description of the ME process, assumed as the results of two independent energy deposits of E_{er} and $E_{n\ell}$, and find that the calculated exclusion limits are indistinguishable. Furthermore, we assume that the NR and ME electrons are generated simultaneously and independently by the two processes, neglecting the possible interaction of ionization clouds. Finally, the pure NR DM signal con-

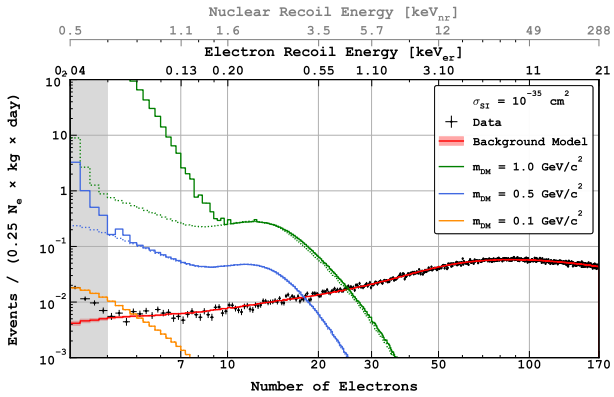


FIG. 2. Data (black) and background model (red) after the selection and fit described in [40]. The expected spectra including the Migdal effect assuming a spin independent DM-nucleon scattering cross section of 10^{-35} cm^2 and DM masses of 0.1, 0.5 and 1.0 GeV/c^2 are shown in orange, blue and green. The gray shaded band shows the S2 threshold used in the analysis.

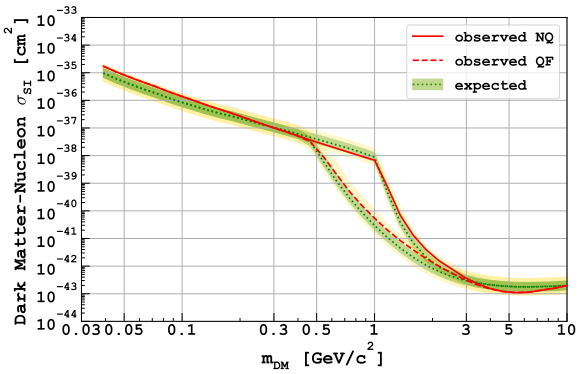


FIG. 3. Upper limits at 90 % C.L. on the spin independent DM - nucleon cross section from the DS-50 experiment considering the Migdal effect. The observed NQ (QF) and the expected limits are shown by the solid (dashed) red curve and the dotted green curve, respectively. The $\pm1\sigma$ and $\pm2\sigma$ expected limits are shown as the green and yellow shaded bands respectively.

tribution is summed with the ME contribution to obtain the total signal spectrum. The fraction of NR events where the ME occurs increases as the DM mass increases. As an example, these fractions are 2.9×10^{-5} at 100 MeV/c^2 and 1.2×10^{-3} at 1 GeV/c^2.

Figure 2 shows the comparison between the predicted dark matter signal (orange, blue and green lines), the DS-50 data (black points) and the fit of the background model (red curve). The signal shown was produced for a spin independent scattering cross section $\sigma_{DM} = 10^{-35}$ cm^2 and different dark matter masses (orange for $m_{DM} = 0.1$ GeV/c^2, blue for $m_{DM} = 0.5$ GeV/c^2 and green for $m_{DM} = 1.0$ GeV/c^2). Given our uncertainties on how to model the size of the fluctuations of the ionization distribution of nuclear recoils, we consider two separate models. The first one (QF) allows for fluctuations in the ionization yield, recombination process and energy quenching modeled via binomial distributions. These fluctuations, for DM masses yielding events around or below the experimental threshold of $N_e = 4$, are significant given the small number of electrons. The second model (NQ) sets the fluctuations in energy quenching to zero. The solid lines are obtained assuming the QF model, while the dotted ones correspond to the NQ model. The signal rate for $m_{DM} = 1.0$ GeV/c^2 contains contributions from NR and ME which are both above the analysis threshold when the quenching fluctuations are included, with the two contributions competing in order to set the limit. On the other hand, the distributions for $m_{DM} = 0.5$ and 0.1 GeV/c^2 are dominated above threshold solely by the ME, independently of the fluctuation model chosen.

The S2 observed energy spectrum is interpreted using a binned profile likelihood as described in detail in [40]. The bins are assumed independent of each other and in each bin the probability is described by a Poisson distribution. The Poisson intensity parameter of the i-th bin is given by the sum of the signal contribution, multiplied by its normalization parameter, and the expected background templates. These quantities are affected by the uncertainties on the exposure, ionization energy scale, the estimate of the radioactivity present in the detector, and the theoretical spectral shapes. Such systematic effects are implemented by means of a set of nuisance parameters that acts on the normalizations and spectral shapes of the background and signal spectra. This likelihood has been used to perform a background-only fit in the region $N_e = [4, 170]$, resulting in a good description of the observed spectrum as shown by the red histogram of Figure 2. The post-fit values of the nuisance parameters are in good agreement with the nominal ones [40], confirming the reliability of the fit.

The search for spin independent dark matter-nucleon interactions via the ME is performed with a profile log-likelihood ratio test statistic based on the above likelihood function and the dark matter signal described in the previous paragraphs. The observed limit at 90% C.L. for the NQ (QF) signal model is shown as a solid (dashed) red curve in Figure 3, together with the corresponding $\pm1\sigma$ (green shaded area) and $\pm2\sigma$ (yellow shaded area) expected limits. The observed limit is compatible within 1σ with the expected one, showing no significant excess

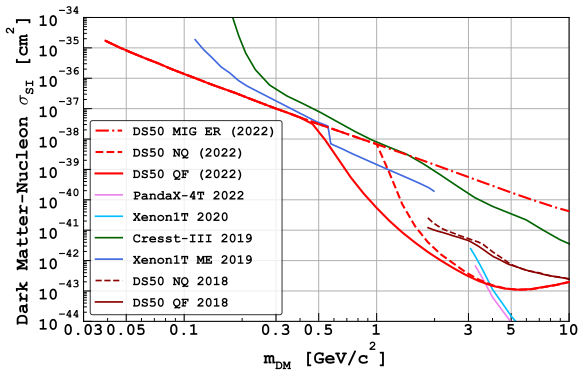


FIG. 4. Upper limits on the spin independent DM-nucleon cross section at 90% C.L. obtained with a signal including the Migdal effect (red solid, dashed, and dash-dotted curves). Also shown are limits Cresst-III (green) [49], Xenon1T (light and dark blue) [33, 50] and DS-50 (dark red) [36]. Other weaker limits [6, 8, 51–57] and claimed discovery [58–61] are not shown.

above the expected background in the region above $N_e = 4$. The choice of the fluctuation model affects only the intermediate region between 0.5 and 5 GeV/c^2. Indeed, this is the transition region between a signal that is dominated by the nuclear recoil and one that is dominated by the ME with nuclear recoils just below the analysis threshold.

The observed upper limits presented in this Letter are compared in Figure 4 with other experiments [33, 36, 49, 50, 56]. The limit is entirely driven by the ME for DM masses below 0.5 GeV/c^2. The DS-50 experiment reaches the best sensitivity for the dark matter spin-independent scattering cross section for masses below 3.6 GeV/c^2, improving considerably the sensitivity with respect to the analysis of 2018 [36].

The limits benefit from the extended signal region $N_e \in [4, 170]$ even though the signal rate typically is negligible with respect to the background rate for $N_e > 50$ for masses of $\mathcal{O}(1)$ GeV. The larger N_e region provides further constraints on the calibration parameters, resulting in a stronger limit.

Exploiting data from the full exposure of the DS-50 experiment, we performed a search for LDM by analysing the ionization signals induced by DM particles scattering off nuclei, enhanced by the Migdal effect. The Migdal detection channel, together with the new calibration [39], data selection, and background model [40], improves significantly the sensitivity of DS-50 to spin-independent DM-nucleon interactions for sub-GeV masses. This analysis sets the world best limit on the spin-independent DM-nucleon cross section for masses below 3.6 GeV/c^2 and down to 40 MeV/c^2. With the DarkSide-20k detector under construction at the LNGS [62], we hope to improve on these limits significantly.

The DarkSide Collaboration offers its profound gratitude to the LNGS and its staff for their invaluable technical and logistical support. We also thank the Fermilab Particle Physics, Scientific, and Core Computing Divisions. Construction and operation of the DarkSide-50 detector was supported by the U.S. National Science Foundation (NSF) (Grants No. PHY-0919363, No. PHY-1004072, No. PHY-1004054, No. PHY-1242585, No. PHY-1314483, No. PHY-1314501, No. PHY-1314507, No. PHY-1352795, No. PHY-1622415, and associated collaborative grants No. PHY-1211308 and No. PHY-1455351), the Italian Istituto Nazionale di Fisica Nucleare, the U.S. Department of Energy (Contracts No. DE-FG02-91ER40671, No. DEAC02-07CH11359, and No. DE-AC05-76RL01830), the Polish NCN (Grant No. UMO-2014/15/B/ST2/02561) and the Foundation for Polish Science (Grant No. Team2016-2/17). We also acknowledge financial support from the French Institut National de Physique Nucléaire et de Physique des Particules (IN2P3), the IN2P3-COPIN consortium (Grant No. 20-152), and the UnivEarthS LabEx program (Grants No. ANR-10-LABX-0023 and No. ANR-18-IDEX-0001), from the São Paulo Research Foundation (FAPESP) (Grant No. 2016/09084-0), from the Interdisciplinary Scientific and Educational School of Moscow University "Fundamental and Applied Space Research", from the Program of the Ministry of Education and Science of the Russian Federation for higher education establishments, project No. FZWG-2020-0032 (2019-1569), from IRAP AstroCeNT funded by FNP from ERDF, and from the Science and Technology Facilities Council, United Kingdom. This project has received funding from the European Union's Horizon 2020 research and innovation program under grant agreement No 952480. Isotopes used in this research were supplied by the United States Department of Energy Office of Science by the Isotope Program in the Office of Nuclear Physics.

[1] V. C. Rubin, N. Thonnard, and W. K. Ford, Jr., Astrophys. J. **238**, 471 (1980).
[2] D. Clowe, A. Gonzalez, and M. Markevitch, Astrophys. J. **604**, 596 (2004), arXiv:astro-ph/0312273.
[3] N. Aghanim *et al.* (Planck), Astron. Astrophys. **641**, A6 (2020), [Erratum: Astron.Astrophys. 652, C4 (2021)], arXiv:1807.06209 [astro-ph.CO].

[4] G. Jungman, M. Kamionkowski, and K. Griest, Phys. Rept. **267**, 195 (1996), arXiv:hep-ph/9506380.
[5] P. Agnes *et al.* (DarkSide), Phys. Rev. D **93**, 081101 (2016), [Addendum: Phys.Rev.D 95, 069901 (2017)], arXiv:1510.00702 [astro-ph.CO].
[6] D. S. Akerib *et al.* (LUX), Phys. Rev. Lett. **118**, 021303 (2017), arXiv:1608.07648 [astro-ph.CO].
[7] X. Cui *et al.* (PandaX-II), Phys. Rev. Lett. **119**, 181302 (2017), arXiv:1708.06917 [astro-ph.CO].
[8] E. Aprile *et al.* (XENON), Phys. Rev. Lett. **121**, 111302 (2018), arXiv:1805.12562 [astro-ph.CO].
[9] R. Essig *et al.*, in *Community Summer Study 2013: Snowmass on the Mississippi* (2013) arXiv:1311.0029 [hep-ph].
[10] M. Battaglieri *et al.*, in *U.S. Cosmic Visions: New Ideas in Dark Matter* (2017) arXiv:1707.04591 [hep-ph].
[11] A. Migdal, J. Phys. USSR **4**, 449 (1941).
[12] T. Ruijgrok, B. Nijboer, and M. Hoare, Physica A: Statistical Mechanics and its Applications **120**, 537 (1983).
[13] L. Vegh, Journal of Physics B: Atomic and Molecular Physics **16**, 4175 (1983).
[14] G. Baur, F. Rosel, and D. Trautmann, Journal of Physics B: Atomic and Molecular Physics **16**, L419 (1983).
[15] P. Sharma, Nucl. Phys. A **968**, 326 (2017).
[16] R. Bernabei *et al.*, Int. J. Mod. Phys. A **22**, 3155 (2007), arXiv:0706.1421 [astro-ph].
[17] M. Ibe, W. Nakano, Y. Shoji, and K. Suzuki, JHEP **03**, 194, arXiv:1707.07258 [hep-ph].
[18] M. J. Dolan, F. Kahlhoefer, and C. McCabe, Phys. Rev. Lett. **121**, 101801 (2018), arXiv:1711.09906 [hep-ph].
[19] N. F. Bell, J. B. Dent, J. L. Newstead, S. Sabharwal, and T. J. Weiler, Phys. Rev. D **101**, 015012 (2020), arXiv:1905.00046 [hep-ph].
[20] D. Baxter, Y. Kahn, and G. Krnjaic, Phys. Rev. D **101**, 076014 (2020), arXiv:1908.00012 [hep-ph].
[21] R. Essig, J. Pradler, M. Sholapurkar, and T.-T. Yu, Phys. Rev. Lett. **124**, 021801 (2020), arXiv:1908.10881 [hep-ph].
[22] Z.-L. Liang, L. Zhang, F. Zheng, and P. Zhang, Phys. Rev. D **102**, 043007 (2020), arXiv:1912.13484 [cond-mat.mes-hall].
[23] G. Grilli di Cortona, A. Messina, and S. Piacentini, JHEP **11**, 034, arXiv:2006.02453 [hep-ph].
[24] C. P. Liu, C.-P. Wu, H.-C. Chi, and J.-W. Chen, Phys. Rev. D **102**, 121303 (2020), arXiv:2007.10965 [hep-ph].
[25] U. K. Dey, T. N. Maity, and T. S. Ray, Phys. Lett. B **811**, 135900 (2020), arXiv:2006.12529 [hep-ph].
[26] S. Knapen, J. Kozaczuk, and T. Lin, Phys. Rev. Lett. **127**, 081805 (2021), arXiv:2011.09496 [hep-ph].
[27] N. F. Bell, J. B. Dent, B. Dutta, S. Ghosh, J. Kumar, and J. L. Newstead, Phys. Rev. D **104**, 076013 (2021), arXiv:2103.05890 [hep-ph].
[28] J. F. Acevedo, J. Bramante, and A. Goodman, Phys. Rev. D **105**, 023012 (2022), arXiv:2108.10889 [hep-ph].
[29] W. Wang, K.-Y. Wu, L. Wu, and B. Zhu, (2021), arXiv:2112.06492 [hep-ph].
[30] D. S. Akerib *et al.* (LUX), Phys. Rev. Lett. **122**, 131301 (2019), arXiv:1811.11241 [astro-ph.CO].
[31] E. Armengaud *et al.* (EDELWEISS), Phys. Rev. D **99**, 082003 (2019), arXiv:1901.03588 [astro-ph.GA].
[32] Z. Z. Liu *et al.* (CDEX), Phys. Rev. Lett. **123**, 161301 (2019), arXiv:1905.00354 [hep-ex].
[33] E. Aprile *et al.* (XENON), Phys. Rev. Lett. **123**, 241803 (2019), arXiv:1907.12771 [hep-ex].
[34] G. Adhikari *et al.* (COSINE-100), (2021), arXiv:2110.05806 [hep-ex].
[35] P. Agnes *et al.* (DarkSide), Phys. Lett. B **743**, 456 (2015), arXiv:1410.0653 [astro-ph.CO].
[36] P. Agnes *et al.* (DarkSide), Phys. Rev. Lett. **121**, 081307 (2018), arXiv:1802.06994 [astro-ph.HE].
[37] P. Agnes *et al.* (DarkSide), Phys. Rev. D **98**, 102006 (2018), arXiv:1802.07198 [astro-ph.CO].
[38] P. Agnes *et al.* (DarkSide), Phys. Rev. Lett. **121**, 111303 (2018), arXiv:1802.06998 [astro-ph.CO].
[39] P. Agnes *et al.* (DarkSide), Phys. Rev. D **104**, 082005 (2021), arXiv:2107.08087 [physics.ins-det].
[40] P. Agnes *et al.* (DarkSide Collaboration), Manuscript submitted to Phys. Rev. D (2022).
[41] M. Wang, W. J. Huang, F. G. Kondev, G. Audi, and S. Naimi, Chin. Phys. C **45**, 030003 (2021).
[42] F. Bezrukov, F. Kahlhoefer, M. Lindner, F. Kahlhoefer, and M. Lindner, Astropart. Phys. **35**, 119 (2011), arXiv:1011.3990 [astro-ph.IM].
[43] J. P. Biersack and J. F. Ziegler, in *Ion Implantation Techniques*, edited by H. Ryssel and H. Glawischnig (Springer Berlin Heidelberg, Berlin, Heidelberg, 1982) pp. 122–156.
[44] H. Cao *et al.* (SCENE), Phys. Rev. D **91**, 092007 (2015), arXiv:1406.4825 [physics.ins-det].
[45] P. Agnes *et al.*, Phys. Rev. D **97**, 112005 (2018), arXiv:1801.06653 [physics.ins-det].
[46] T. H. Joshi *et al.*, Phys. Rev. Lett. **112**, 171303 (2014), arXiv:1402.2037 [physics.ins-det].
[47] D. Baxter, I. M. Bloch, E. Bodnia, X. Chen, J. Conrad, P. Di Gangi, J. E. Y. Dobson, D. Durnford, S. J. Haselschwardt, A. Kaboth, R. F. Lang, Q. Lin, W. H. Lippincott, J. Liu, A. Manalaysay, C. McCabe, K. D. Morå, D. Naim, R. Neilson, I. Olcina, M. C. Piro, M. Selvi, B. von Krosigk, S. Westerdale, Y. Yang, and N. Zhou, The European Physical Journal C **81**, 907 (2021).
[48] R. Catena, T. Emken, N. A. Spaldin, and W. Tarantino, Phys. Rev. Res. **2**, 033195 (2020), arXiv:1912.08204 [hep-ph].
[49] A. H. Abdelhameed *et al.* (CRESST), Phys. Rev. D **100**, 102002 (2019), arXiv:1904.00498 [astro-ph.CO].
[50] E. Aprile *et al.* (XENON), Phys. Rev. Lett. **123**, 251801 (2019), arXiv:1907.11485 [hep-ex].
[51] R. Agnese *et al.* (SuperCDMS), Phys. Rev. Lett. **112**, 041302 (2014), arXiv:1309.3259 [physics.ins-det].
[52] G. Angloher *et al.* (CRESST), Eur. Phys. J. C **76**, 25 (2016), arXiv:1509.01515 [astro-ph.CO].

[53] E. Behnke *et al.*, Astropart. Phys. **90**, 85 (2017), arXiv:1611.01499 [hep-ex].
[54] C. Amole *et al.* (PICO), Phys. Rev. Lett. **118**, 251301 (2017), arXiv:1702.07666 [astro-ph.CO].
[55] R. Agnese *et al.* (SuperCDMS), Phys. Rev. D **97**, 022002 (2018), arXiv:1707.01632 [astro-ph.CO].
[56] Y. Meng *et al.* (PandaX-4T), Phys. Rev. Lett. **127**, 261802 (2021), arXiv:2107.13438 [hep-ex].
[57] M. Traina *et al.* (DAMIC), PoS **ICRC2021**, 539 (2021), arXiv:2108.05983 [astro-ph.CO].
[58] C. E. Aalseth *et al.* (CoGeNT), Phys. Rev. Lett. **106**, 131301 (2011), arXiv:1002.4703 [astro-ph.CO].
[59] G. Angloher *et al.*, Eur. Phys. J. C **72**, 1971 (2012), arXiv:1109.0702 [astro-ph.CO].
[60] R. Agnese *et al.* (CDMS), Phys. Rev. Lett. **111**, 251301 (2013), arXiv:1304.4279 [hep-ex].
[61] R. Bernabei *et al.*, Eur. Phys. J. C **73**, 2648 (2013), arXiv:1308.5109 [astro-ph.GA].
[62] C. E. Aalseth *et al.* (DarkSide-20k), Eur. Phys. J. Plus **133**, 131 (2018), arXiv:1707.08145 [physics.ins-det].